International Journal of GEOMATE, Oct., 2021, Vol.21, Issue 86, pp.23-31
ISSN: 2186-2982 (P), 2186-2990 (O), Japan, DOI: https://doi.org/10.21660/2021.86.j2210
Geotechnique, Construction Materials and Environment

QUICK EARTHQUAKE DAMAGE EVALUATION METHOD FOR RC PIERS USING ACCELERATION MEASUREMENTS

*Aiko Furukawa[1], Kazuho Hagiwara[1], Yoshikazu Takahashi[2] and Junji Kiyono[1]

[1]Department of Urban Management, Kyoto University, Japan
[2]Department of Civil and Earth Resources Engineering, Kyoto University, Japan

*Corresponding Author, Received: 21 May 2021, Revised: 11 July 2021, Accepted: 23 Sept. 2021

ABSTRACT: This study proposed a quick earthquake damage evaluation method for RC piers using the short-time transfer function (STTF) obtained from acceleration measurements. This research aims to confirm whether the damage occurrence can be detected from the STTF and the damage degree (maximum displacement) can be estimated from the predominant frequency of the STTF. First, the method was applied to the shaking table test results. The predominant frequency decreased when the crack of concrete or the yielding of the reinforcing bar occurred. Therefore, it was confirmed that the damage occurrence could be detected as the reduction of the predominant frequency. The lowest predominant frequency during excitation was sensitive to the maximum displacement, while the predominant frequency at the end of the exaction was not sensitive to the maximum displacement. The method was also applied to the numerical analysis results. In conclusion, it was confirmed that the method could detect damage occurrence, damage progress, and non-occurrence of damage progress from the transition of the predominant frequency. Also, it was found that the maximum displacement is proportional to the square of the ratio of the initial predominant frequency to the lowest predominant frequency. The possibility to estimate the maximum displacement from the lowest predominant frequency was illustrated.

Keywords: Quick Earthquake Damage Evaluation, RC Pier, Acceleration, Short-Time Transfer Function, Maximum Displacement

1. INTRODUCTION

When a large earthquake occurs, road bridges play an important role in emergency repair and rescue activities. Once the road bridge suffers damage, appropriate and smooth implementation of emergency response cannot be operated. Therefore, quick damage evaluation and quick repair are essential. Usually, earthquake damage is evaluated by visual inspection, but it lacks speed and quantitative criteria for damage evaluation.

The bridge pier is the weakest member among bridge components against horizontal excitation of earthquakes. Therefore, it is necessary to develop a method that can quickly detect and quantify the damage to the bridge pier. In the past decades, vibration-based damage evaluation methods using accelerometers have attracted attention.

Conventionally, the vibration-based damage evaluation method uses the fact that structural damage usually causes a decrease in structural stiffness, thereby producing a reduction in natural frequencies. Therefore, a reduction in natural frequency is estimated by acceleration measurement and used to detect damage occurrence [1][2]. However, it is difficult to quantify the damage degree from the natural frequency.

In past research, the earthquake damage degree was evaluated based on the maximum displacement [3] or the linear function of the maximum displacement and the absorbed hysteretic energy [4]. However, direct measurement of displacement is very difficult in large-scale structures such as road bridges because displacement transducers require fixed reference points that are rarely available [5]. Moreover, the reference points also vibrate during severe earthquakes, so the direct measurement of displacement becomes almost impossible [6]. Measurement of hysteretic energy is far more difficult since it requires a force-displacement relationship.

As an alternative to direct displacement measurements, displacement may be indirectly obtained by time integrations from acceleration measurements. Several types of research evaluated the maximum displacement from acceleration measurements since acceleration is easily measured without a fixed reference point. Various digital filters were used in various applications [6][7]. However, the conventional digital filters have several drawbacks in the displacement reconstruction for structures with low dominant frequency [6]. The method was proposed to accurately predict velocity and displacement from noise-contaminated acceleration and displacement measurements [8]. However, the measurement of displacement itself is difficult.

Methods to estimate the maximum ductility factor from acceleration measurements also have been studied. Kobayashi et al. [9] used the natural periods before and after the earthquake. They estimated the maximum ductility factor as the square of the natural period ratio before and after the earthquake. Their method assumes that the RC piers follow the perfect elastoplastic model with origin-oriented hysteresis characteristics. However, there is no guarantee that the RC piers follow such a hysteresis model. Similar research is also conducted assuming that the RC piers follow the bilinear model with Masing's law [10].

Recently, damage detection methods using time-frequency analysis have been studied. The short-time Fourier transform (STFT) [11], Wavelet transform (WT) [11][12], Hilbert transform (HT) [13], Wigner-Ville distribution (WVD) [14] have been introduced. The time-frequency analysis is used to find the instantaneous spikes in acceleration responses generated by the damage occurrence [12] or to estimate the temporal change of frequency characteristics of structures during earthquakes [14].

In most past research on the time-frequency analysis methods, the main objective is to verify whether the instantaneous predominant frequency can be detected and a decrease of frequency can be captured. The detected predominant frequency has not been related to the degree of damage, such as the maximum displacement or maximum ductility factor.

With this background, this paper introduces the short-time transfer function (STTF) for quick earthquake damage evaluation of RC pier. The STTF is obtained as the ratio of the STFT of two acceleration measurements at the girder (pier top) and the footing (pier bottom). The first objective is to investigate whether the STTF can capture the transition of predominant frequency of an RC pier during small to large earthquake excitations, and damage can be detected from the transition of the predominant frequency. The second objective is to investigate whether the predominant frequency can be related to the maximum displacement, quantifying the degree of damage. The proposed method is verified using the shaking table results and the numerical analysis results.

2. PROPOSED METHOD

2.1 Procedure of Proposed Method (Fig. 1)

The target structure is an RC pier composed of a footing, a pier, and a girder, as shown in Fig. 1. It is assumed that two accelerometers are installed at the footing and the girder, and horizontal accelerations are measured. The acceleration measured at the footing is defined as input acceleration, and the acceleration measured at the girder is defined as response acceleration.

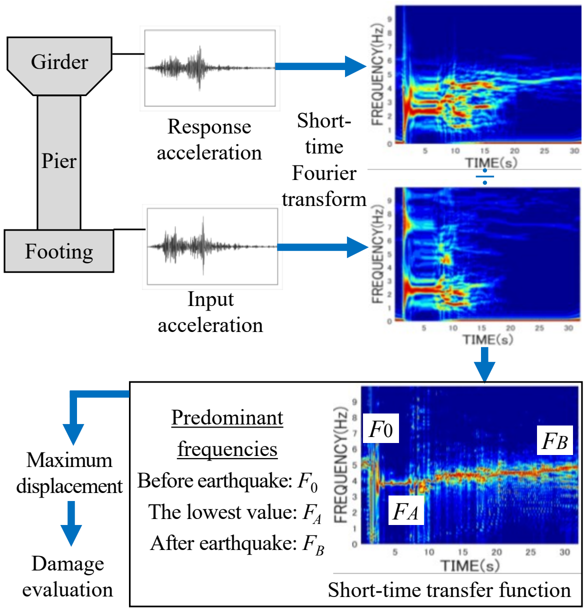

Fig. 1. The procedure of quick damage detection

The procedure of the proposed method is as follows. At step 1, input and response accelerations are measured during an earthquake. At step 2, the method computes the short-time Fourier transforms (STFT) of the accelerations. The STFT provides the time-localized frequency information, such as which frequency is predominant at which time [15].

At step 3, the method computes the short-time transfer function (STTF) by dividing the STFT of the response acceleration by the STFT of the input acceleration. The contour values of Fig. 1 are normalized so that the maximum value becomes 1 for each time step. The blue indicates 0, and the red indicates 1. The red color shows the predominant frequency for each time step.

At step 4, the method extracts the initial predominant frequency before the earthquake F_0 (intact state), the lowest predominant frequency during the earthquake F_A, and the predominant frequency at the end of the earthquake F_B from the STTF.

The method relates the predominant frequencies to the damage-related index (maximum displacement). As the last step, the damage degree is evaluated from the predominant frequencies.

2.2 Comparison with Past Research [9]

In the past research [9], the maximum ductility factor (damage-related index) μ is estimated as

$$\mu = (T_d/T)^2 \tag{1}$$

where T and T_d are the natural periods before and after the earthquake. Eq. (1) is rewritten using the predominant frequencies as

$$\mu = (F_0/F_B)^2 \tag{2}$$

(a) 16 RC piers on the shaking table

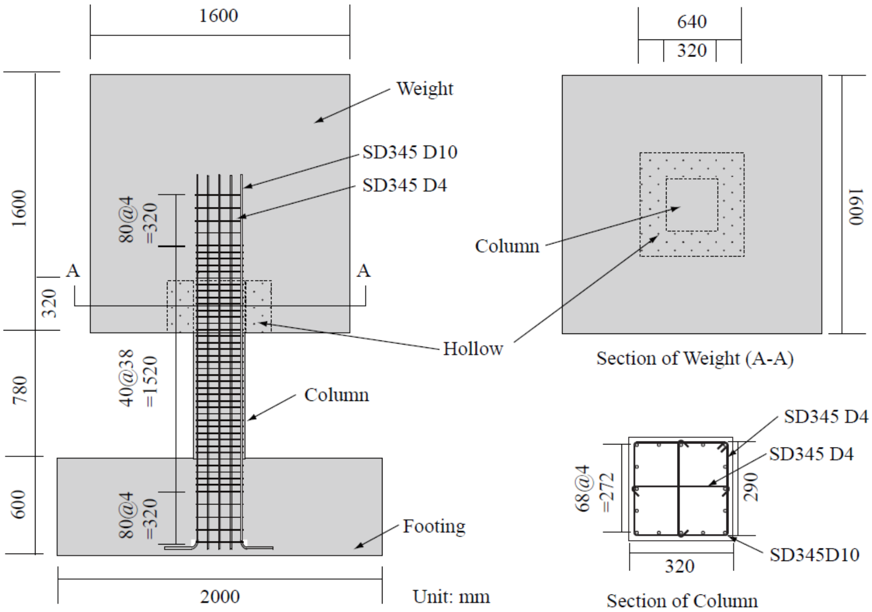

(b) Design drawing of RC pier

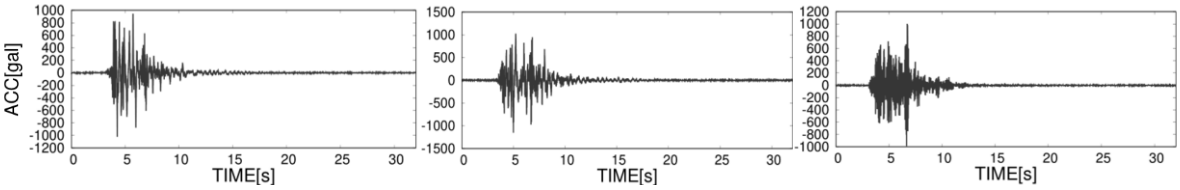

(c) Measured acceleration on the footing during the JR Takatori wave of 100% (1) (X, Y, and Z from the left)

Fig. 2. Shaking table test

where F_0 and F_B are the predominant frequencies at the beginning and at the end of the earthquake. The lowest predominant frequency F_A is not used [9].

Eq.(1) is derived assuming that the RC pier follows an origin-oriented perfectly elastoplastic model. Therefore, Eq.(1) cannot correctly estimate the maximum ductility factor when the assumption is not satisfied.

3. EXPERIMENTAL VERIFICATION

3.1 Shaking Table Test [16]

3.1.1 Shaking table test

The proposed method was applied to the shaking table test results of RC piers [16] (Fig.2(a)). 16 RC piers were manufactured under the same design, numbered from specimen 01 to 16, and simultaneously excited on the shaking table. The original aim of this test was to quantitatively evaluate the variations of the nonlinear behaviors among 16 piers. The design drawing of the RC pier is shown in Fig. 2(b). It is a 1/7.5 scale model of a full-scale RC pier.

3.1.2 Input acceleration

Table 1 shows the input acceleration cases. The case name defined in Table 1 will be used to indicate the excitation case. The specimen was firstly excited with random waves with small amplitude to understand the linear vibration characteristics.

Table 1. Input acceleration case

Order	Case name	Wave name	Amplitude adjusted ratio	Observed phenomena
1	Random(1)	Random wave with small amplitude		Linear behavior
2	Random(2)			
3	Random(3)			
4	12.5%	Amplitude adjusted JR Takatori wave	12.5%	Nonlinear behavior with small plastic deformation (Crack of concrete occurred.)
5	18.75%		18.75%	
6	10%		10%	
7	15%		15%	
8	18%(1)		18%(1st)	
9	18%(2)		18%(2nd)	
10	100%(1)		100%(1st)	Nonlinear behavior with large plastic deformation (Yielding of reinforcing bar occurred.)
11	100%(2)		100% (2nd, X and Y components were inverted.)	
12	150%		150%	

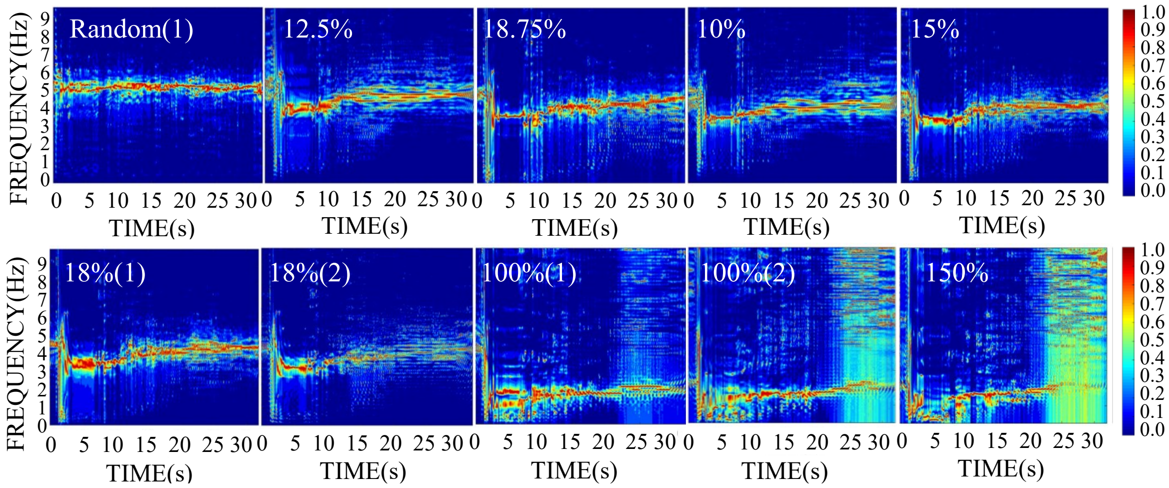

(a) Short-time transfer functions (X direction)

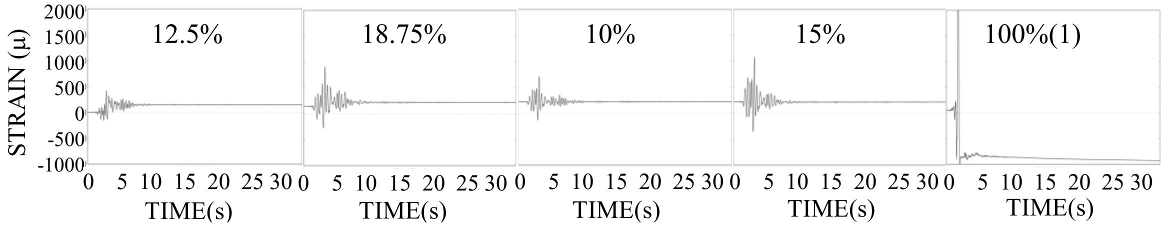

(b) Strain history

Fig. 3. Short-time transfer function (STTF) and strain history of Specimen 01

Table 2. Predominant frequencies (Hz)

Case name	The predominant frequency at intact state F_0	The lowest predominant frequency F_A	The predominant frequency at the end of excitation F_B
12.5%	5.7	3.9	5.0
18.75%		3.7	4.5
10%		3.8	4.4
15%		3.8	4.4
18%(1)		3.4	4.3
18%(2)		3.2	4.4
100%(1)		0.98	2.2
100%(2)		0.88	2.1
150%		0.78	2.1

Then the amplitude-adjusted JR Takatori waves were input in sequence. JR Takatori wave is an acceleration record observed at the Takatori Station during the 1995 Hyogo-ken Nanbu Earthquake. Since the specimen is 1/7.5 scale, the time axis of the acceleration record was compressed $1/\sqrt{7.5}$ times according to the scaling law [17]. The positive directions of the X, Y, and Z-axes were set to the north, west, and upward. The acceleration amplitude was adjusted from 10% to 150%. The acceleration observed on the footing for the case of 100%(1) is shown in Fig. 2(c).

3.1.3 Shaking table test results

The observed phenomena are summarized in Table 1. The specimen showed linear behavior during the random wave excitation. Cracks of concrete occurred, and nonlinear behavior with small plastic deformation was observed from 12.5% to 18%(2). Yielding of reinforcing bar occurred, and nonlinear behavior with large plastic deformation was observed after 100%(1). The yielding of the reinforcing bar was recognized from the strain gauge value of the reinforcing bar. Since the 16 specimens showed similar results, and the same tendency was observed in both the X and Y directions, this study will deal with the results of specimen 01 in the X-direction.

3.2 Computation Condition of STTF

The measured input and response accelerations have a time interval of 0.005 sec and a duration of 32 sec. In the STFT, a rectangular window function with a time width of 5 sec was used. The Fourier spectrum was smoothed using a Parzen window with a width of 0.2 Hz. The STTF was standardized so that the maximum value for each time step becomes 1. As for the time window, 5 sec was selected since it is the minimum time width that can capture the predominant frequency.

3.3 STTF and Predominant Frequency Transition

Figure 3(a) shows the computed STTF of specimen 01 in the X direction for a series of excitation. The red color indicates the frequency with the highest amplitude at each time. It is possible to capture the transition of the predominant frequency by tracking the red color. The predominant frequency is continuous during a series of excitation. Table 2 indicates the lowest predominant frequency F_A and the predominant frequency at the end of the excitation F_B of each excitation case.

3.3.1 Random wave excitation

In the STTF of the 1st random wave excitation (Fig. 3(a)), the predominant frequency is almost constant at about 5.7 Hz, which means that the specimen showed linear behavior. The predominant frequency at intact state F_0 was found to be 5.7 Hz.

3.3.2 JR Takatori wave excitation of 12.5%

In the STTF of 12.5% (Fig. 3(a)), the predominant frequency is about 5.7 Hz at the beginning, dropped rapidly at about 2.5 sec, reached the minimum value of about 3.9 Hz (F_A), then gradually increased, and finally reached about 5.0Hz (F_B). Since the STTF at 2.5sec is the transfer function from 0 to 5 sec, the occurrence of nonlinear behavior at 5.0 Hz appeared in the STTF at 2.5 sec.

Figure 3(b) shows the strain history measured by the strain gauge installed to the reinforcing bar in the southwest corner at the height of 100mm. To compare the time axis between STTF and strain history, the time axis of strain was shifted 2.5 sec earlier. From the strain history, the occurrence of residual strain is observed. The strain value is smaller than the yield strain of the reinforcing bar and close to the yield strain of the concrete. Therefore, the cause of the residual strain is the stress redistribution due to a crack occurrence in the concrete.

The occurrence of crack can be detected by the decrease of the predominant frequency of the STTF.

3.3.3 JR Takatori wave excitation of 18.75%

Both F_A and F_B of 18.75% were lower than those of 12.5%, indicating the damage progress (Fig. 3(a), Table 2). The slight increase in the residual strain (Fig. 3(b)) is evidence of the crack progress. The damage progress can be detected by the predominant frequency of the STTF.

3.3.4 JR Takatori wave excitation of 10% and 15%

The input acceleration amplitudes for 10% and 15% are smaller than that of 18.75%. So, it is expected that damage did not progress. To support this, F_A and F_B of these cases are similar to those of 18.75% (Fig.3(a), Table 2). The residual strain also did not increase and supported the assumption that the progress of damage did not occur (Fig. 3(b)). It was found that the STTF can detect the non-occurrence of damage progress.

3.3.5 JR Takatori wave excitation of 18%(1) and (2)

In the STTFs of 18%(1) and 18%(2), F_A is lower than and F_B is similar to those of 18.75% (Fig. 3(a), Table 2). It means that F_A suggests the progress of damage while F_B suggests the non-occurrence of damage progress. As will be indicated in the next section, the maximum displacements of these cases were larger than 18.75%. So, the damage may be progressed. Therefore, the predominant frequency F_A is a more sensitive index to detect damage.

3.3.6 JR Takatori wave excitation of 100%(1)

In the STTF of 100%(1) (Fig. 3(a)), the predominant frequency dropped sharply to the minimum value of about 1.0 Hz because the yielding of the reinforcing bar occurred. Fig. 3(b) indicates a large strain of 2000 μ, which is close to the yield strain of the reinforcing bar. Since the reinforcing bar yielded in the case of 100%(1), the predominant frequency decreased largely compared to the cases from 12.5% to 18%(2) with no yielding of the reinforcing bars.

3.3.7 JR Takatori wave excitation of 100%(2) and 150%

In the STTFs of 100%(2) and 150%, F_A is smaller than and F_B is similar to those of 100%(1) (Fig. 3(a), Table 2). From this, it is found that F_A is more sensitive to damage.

3.3.8 Summary

It was confirmed that the transition of the predominant frequency during excitation could be captured by the STTF. It was shown that the lowest predominant frequency F_A is sensitive to damage and can detect the occurrence of concrete cracks, yielding of reinforcing bar, damage progress, and also non-occurrence of damage progress.

3.4 Relationships between Predominant Frequency and Maximum Displacement

The maximum displacement and the maximum ductility factor are often used to evaluate the damage. This study investigates the relationship between the square of the predominant frequency ratio ($(F_0/F_A)^2$, $(F_0/F_B)^2$) and the maximum displacement for each excitation case. The predominant frequency at the intact state (5.7Hz) is input to F_0.

Fig. 4(a) shows the relationship between $(F_0/F_A)^2$ and the maximum displacement. The result for all cases is on the left side, and that from 12.5% to 18%(2) is on the right side. An almost linear relationship was observed.

Fig. 4(b) shows the relationship between $(F_0/F_B)^2$ and the maximum displacement. The linear relationship was not observed. It was found that Eq.(1) or (2) is not appropriate for the shaking table test results in this study.

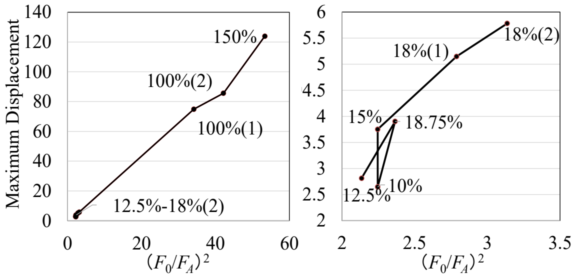

(a) The lowest predominant frequency F_A

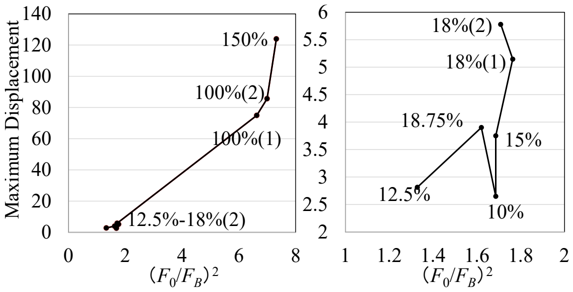

(b)Predominant frequency at the end of excitation F_B

Fig. 4. Relationship between the predominant frequencies and maximum displacement (mm)

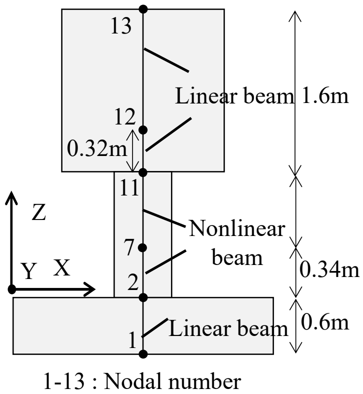

(a)Numerical model

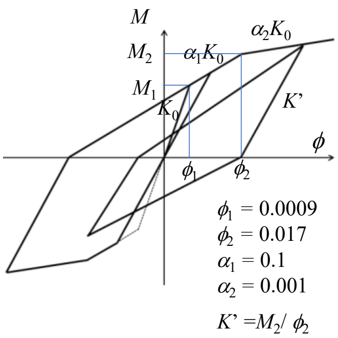

(b)Moment-curvature relationship

Fig. 5. Numerical model and constitutive models

Table 3. Material properties

Member	Density (kg/m^3)	Young's modulus (N/m^2)	Poisson's ratio	Shear section modulus
Pier	2.5×10^3	4.75×10^{10}	0.2	1.2
Footing/Girder	2.5×10^3	4.75×10^{12}	0.2	1.2

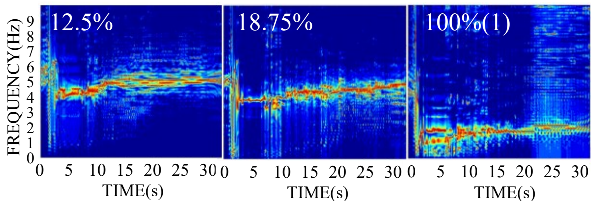

(a) Shaking table test results

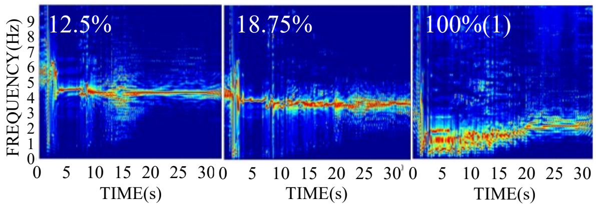

(b) Analysis results

Fig. 6. Comparison of the STTFs

From 12.5% to 18%(2), the maximum displacement increased from 2.81 mm to 5.78 mm. The increase of $(F_0/F_A)^2$ and $(F_0/F_B)^2$ was 0.34 and 0.13 for a 1mm increase of the maximum displacement. From 100%(1) to 150%, the maximum displacement increased from 74.9 mm to 123.9 mm. The increase of $(F_0/F_A)^2$ and $(F_0/F_B)^2$ was 0.39 and 0.014 for a 1mm increase of the maximum displacement. The increase of $(F_0/F_B)^2$ becomes drastically small as the large maximum displacement increases.

The above shows that $(F_0/F_A)^2$ is a better index to estimate the maximum displacement.

4. NUMERICAL VERIFICATION

4.1 Numerical Model

Since the previous chapter was limited to the amplitude-adjusted JR Takatori waves, this chapter numerically verifies the proposed method using different earthquake ground motions.

The seismic behavior of the shaking table test specimen was simulated by the finite element analysis. The specimen was modeled using the Timoshenko beam, as shown in Fig. 5(a). The pier was modeled with nonlinear elements. The footing and the girder were modeled with linear elements. Node 1 was fixed for 6 degrees of freedom.

Table 3 shows the material properties. Young's modulus of the pier was determined from the element test results [16]. The density was estimated so that the first mode natural frequency matches the predominant frequency at the intact state (F_0 = 5.7Hz) of the experiment. General value was used for Poisson's ratio. The Young's modulus of the footing and the girder was set large, assuming that they are rigid. The cross-sectional area, the second moment of the area, and the shear section modulus were determined based on the design drawing shown in Fig. 2(a).

The degrading trilinear (Mutoh) model was used for the moment-curvature relationship of the pier (Fig.5(b)). The first and the second breaking points correspond to the crack of concrete and the yielding of the reinforcing bar. When the maximum curvature is between the first and the second breaking point, it shows the origin-oriented hysteresis characteristics. When the curvature exceeds the second breaking point, it shows the maximum-oriented hysteresis characteristics.

Rayleigh damping was adopted. Damping factors for 5.7Hz and 1.0 Hz were set 5% so that the damping factor for the predominant frequency during excitation becomes about 5%.

Newmark's β method (β=1/4) was used for numerical time integration. The computation time interval is 0.005 sec.

4.2 Verification of Numerical Model

4.2.1 Analytical condition

The accelerations measured on the footing of specimen 01 for cases from 12.5% to 150% were connected. It was input into the numerical model, and the response acceleration at Node 12 was computed and divided for each excitation case. The STTF was computed for each excitation case. h

4.2.2 Comparison between experiment and analysis

Figure 6 shows a comparison of the STTFs. Results for 12.5%, 18.75%, and 100% (1) are shown as examples.

First, the comparison is made for 12.5% and 18.75%, where only cracking of concrete occurred. In the experiment, the predominant frequency decreased then gradually increased. The predominant frequency of the analysis decreased simultaneously as the experiment, but then it kept almost constant. Since the degrading trilinear model shows origin-oriented characteristics up to the second breaking point, the predominant frequency was kept constant.

Table 4. Input ground motions

Type name	Earthquake type	Soil profile type	Observation point
Type I-I	Interplate earthquake (The 2011 off the Pacific coast of Tohoku Earthquake)	Type I (Hard)	Touwa (K-NET MYG003)
Type I-II		Type II (Medium)	Toyosato (K-NET MYG007)
Type I-III		Type III (Soft)	Furukawa (K-NET MYG006)
Type II-I	Intraplate earthquake (1995 Hyogo-ken Nanbu Earthquake)	Type I (Hard)	Kobe Marine Observatory
Type II-II		Type II (Medium)	JR Takatori Station
Type II-III		Type III (Soft)	Higashi Kobe Ohashi Bride

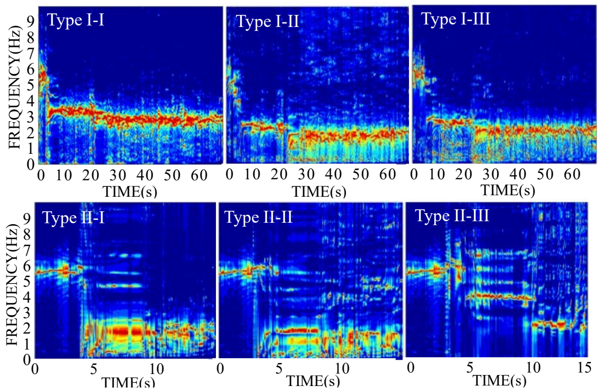

(a) Short-time transfer function

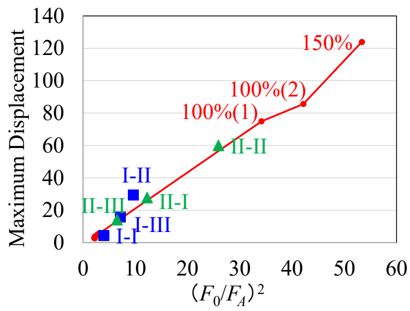

(b)Relationship between the predominant frequency and the maximum displacement (mm)

Fig. 7. Application to different ground motions

Next, the comparison is made for 100% (1), where the yielding of the reinforcing bar occurred. The STTFs of the experimental and analysis look similar. The predominant frequency decreased and then gradually increased. Since the moment-curvature relationship after the second breaking point shows the maximum-oriented hysteresis characteristics, the increase of the predominant frequency could be expressed by the analysis.

It is expected that the analysis accuracy will be improved by modifying the moment-curvature relationship between the first and the second breaking points into the maximum-oriented model.

The increase of the predominant frequency for 12.5% and 18.75% could not be simulated. However, the decrease of the predominant frequency could be simulated by the analysis for all excitation cases.

4.3 Application to Different Ground Motions

4.3.1 Input earthquake ground motion

The proposed method is applied to six earthquake ground motion records shown in Table 4. They were named following the classification of the Japanese specification for highway bridges [18]. Type I-I, Type I-II, and Type I-III are the interpolate earthquake (type I) records observed on hard (I), medium (II), and soft (III) soil. The earthquake records observed during the 2011 off the Pacific coast of Tohoku Earthquake were used [19]. Type

II-I, Type II-II, and Type II-III are the intraplate earthquake (type II) records. The earthquake records observed during the 1995 Hyogo-ken Nanbu earthquake were used.

Since the specimen is 1/7.5 scale, the time axis of the acceleration record was compressed $1/\sqrt{7.5}$ times according to the scaling law. The acceleration records in three directions were input, but only the X direction (NS component) results will be investigated.

4.3.2 Results

The STTFs are shown in Fig. 7(a). The predominant frequency is unclear, but the transition can be read. The predominant frequency did not gradually increase since the yielding of the reinforcing bar did not occur.

Next, Fig. 7(b) shows the relationship between the square of the predominant frequency ratio $(F_0/F_A)^2$ and the maximum displacement. The results for interpolate and intraplate earthquakes are shown with blue and green. The red dotted line indicates the results of the shaking table test. The blue and green marks almost overlapped on the red line. It was confirmed that $(F_0/F_A)^2$ is a highly correlated index with the maximum displacement.

If the criteria for classifying the damage degree from the maximum displacement are prepared for each pier, the damage degree can be evaluated by the STTF.

5. CONCLUSION

This study proposed a quick earthquake damage evaluation method for RC piers using the short-time transfer function (STTF) obtained from acceleration measurements. The validity of the proposed method was verified by the shaking table test results and the numerical analysis of the RC pier.

First, the method was applied to the shaking table test results where the RC pier was excited by JR Takatori waves with various acceleration levels. It was confirmed that the transition of the predominant frequency during excitation could be captured by the STTF. The predominant frequency dropped sharply when the cracking of the concrete or yielding of the reinforcing bar occurred. The lowest predominant frequency F_A was found to be sensitive to damage and could detect the occurrence of concrete cracks, yielding of reinforcing bar, damage progress, and also non-occurrence of damage progress. The maximum displacement was proportional to $(F_0/F_A)^{2,}$ where F_0 is the predominant frequency at the intact state and F_A is the lowest predominant frequency. The maximum displacement was not proportional to $(F_0/F_B)^{2,}$ where F_B is the predominant frequency at the end of the excitation, and $(F_0/F_B)^2$ was not sensitive for large maximum displacement. This suggests the possibility to estimate the maximum displacement from $(F_0/F_A)^2$.

Next, the method was applied to the numerical analysis results with various input ground motions. It was confirmed that the transition of the predominant frequency could be captured by the STTF, and the maximum displacement was proportional to $(F_0/F_A)^2$ irrespective of the input ground motions.

In future work, we would like to establish a method for automatically quantifying the predominant frequency from STTF. Furthermore, we would like to perform more shaking table tests and numerical analysis with various analysis models and various earthquake ground motions to examine the performance of the proposed method.

It may be difficult to install two accelerometers to all existing RC piers at the moment. However, it may be possible to install two accelerometers to important RC piers consisting of important road networks. In addition, as the sensor technology improves and the sensor cost decreases, the applications will be more realistic. The computational cost is also reducing these days, so the quick evaluation of damage is also possible. In a future study, we would like to develop methods to reduce computation time by avoiding the same computation and improving computational efficiency.

6. REFERENCES

[1] El-Bahy, A., Kunnath, S.K., Stone, W.C., Taylor, A.W., Cumulative seismic damage of circular bridge columns: benchmark and low-cycle fatigue tests, ACI Structural Journal, Vol. 96(4), 1999, pp. 633–641.

[2] Kim, T.H., Lee, K.M., Chung, Y.S., Shin, H.M., Seismic damage assessment of reinforced concrete bridge columns, Engineering Structures, Vol. 27(4), 2005, pp. 576–592. https://doi.org/10.1016/j.engstruct.2004.11.016

[3] Gupta, V.K., Nielsen, S.R.K., Kirkegaard, P.H., A preliminary prediction of seismic damage-based degradation in RC structures, Earthquake Engineering and Structural Dynamics, Vol.30, 2001, pp. 981-993. https://doi.org/10.1002/eqe.45

[4] Smyth, A., Wu, M., Multi-rate Kalman filtering for the data fusion of displacement and acceleration response measurements in dynamic system monitoring, Mechanical Systems and Signal Processing, Vol. 21, 2007, pp.706-723. https://doi.org/10.1016/j.ymssp.2006.03.005

[5] Gavin, H.P., Morales, R., Reilly, K., Drift-free integrators. Review of Scientific Instruments, Vol. 69(5), 1998, pp. 2171–2175. https://doi.org/10.1063/1.1148918

[6] Lee, H.S., Hong, Y.H., Park, H.W., Design of an

FIR filter for the displacement reconstruction using measured acceleration in low-frequency dominant structures. International Journal for Numerical Methods in Engineering, Vol. 82, 2010, pp.403-434. https://doi.org/10.1002/nme.2769

[7] Oppenheim, A.V., Schafer, R.W., Discrete-time Signal Processing (3rd edn), Pearson Education Limited. 2013.

[8] Park, Y.J., Ang, A.H-S, Wen, Y.K., Seismic damage analysis and damage-limiting design of R.C. buildings, Civil Engineering Studies, Technical Report, No. SRS-516, University of Illinois, Urbana Champaign, 1984. http://hdl.handle.net/2142/14124

[9] Kobayashi, H., Unjo, S., Kanoh, T., Development of an earthquake damage detection method for bridge structures with accelerating sensor, Proceedings of the JSCE Earthquake Engineering Symposium, Vol.28, 2005, pp. 23-29. (in Japanese) https://doi.org/10.11532/proee2005a.28.23

[10] Furukawa, A., Igarashi, A., Kiyono, J., Estimation of maximum response ductility using equivalent natural period and damping ratio obtained from acceleration response of a nonlinear SDOF system with bilinear hysteresis during earthquakes, Journal of Japan Society of Civil Engineers, Ser. A2 (Applied Mechanics (AM)), Vol. 67(2), 2011, pp. I_801-I_812. (in Japanese) https://doi.org/10.2208/jscejam.67.I_801

[11] Nagarajaiah, S., Basu, B., Output only modal identification and structural damage detection using time frequency and wavelet techniques. Earthquake Engineering and Engineering Vibration, Vol. 8(4), 2009, pp. 583-605. https://doi.org/10.1007/s11803-009-9120-6

[12] Pnevmatikos, N.G., Hatzigeorgiou, G.D., Damage detection of framed structures subjected to earthquake excitation using discrete wavelet analysis. Bulletin of Earthquake Engineering, Vol. 15, 2017, pp. 227-248. https://doi.org/10.1007/s10518-016-9962-z

[13] Roy, T.B., Banerji, S., Panigrahi, S.K., Chourasia, A., Tirca, L., Bagchi, A., A novel method for vibration-based damage detection in structures using marginal Hilbert spectrum. In: Rao, A., Ramanjaneyulu, K. (eds), Recent Advances in Structural Engineering, Vol. 1, 2019, Lecture Notes in Civil Engineering, Vol. 11. Springer, Singapore. https://doi.org/10.1007/978-981-13-0362-3_92

[14] Ge, X., Alexander, N.A., Kashani, M.M., Rapid post-earthquake damage assessment of aging reinforced concrete bridge piers using time-frequency analysis, Structure and Infrastructure Engineering, 2020. https://doi.org/10.1080/15732479.2020.1801769

[15] Kehtamavas, N., Digital Signal Processing System Design: LabVIEW-Based Hybrid Programming (Digital Signal Processing SET), Academic Press, 2008.

[16] Takahashi, Y., Kobayashi, N., Quantitative evaluation of seismic response based on simultaneous excitation of 16 RC columns. Journal of Japan Society of Civil Engineers, Ser. A1, Vol. 72(1), 2016, pp.176-191. (in Japanese) https://doi.org/10.2208/jscejseee.72.176

[17] Harris, H.G., Sabnis, G.M., Structural modeling and experimental techniques (2nd ed.). 1999, CRC Press.

[18] Japan Road Association, Specifications for highway bridge, Part 5, Seismic design. Maruzen, 2017.

[19] NIED, Strong-motion seismograph networks. http://www.kyoshin.bosai.go.jp/kyoshin. [accessed May 21, 2021]